E7.4-10.242

CR-136540

REMOTE SENSING OF OCEAN CURRENT BOUNDARY LAYER
EREP PROJECT 108

December 1973
Contract Number T-4713-B

N74-15046

(E74-10242) REMOTE SENSING OF OCEAN
CURRENT BOUNDARY LAYER Monthly Progress
Report, Dec. 1973 (National Oceanic and
Atmospheric Administration) 32 p HC $3.75
CSCL 08C
Unclas
G3/13 00242

Principle Investigations Management Office
Lyndon B. Johnson Space Center

Z. H. Byrns, Technical Monitor

George A. Maul, Principle Investigator
National Oceanic & Atmospheric Administration
Atlantic Oceanographic & Meteorological Laboratories

MONTHLY REPORT

RELATIONSHIPS BETWEEN ERTS
RADIANCES AND GRADIENTS ACROSS OCEANIC FRONTS

George A. Maul
Atlantic Oceanographic and Meteorological Laboratories
National Oceanic and Atmospheric Administration
Miami, Florida

Howard R. Gordon
Department of Physics
Optical Physics Laboratory, and
Rosenstiel School of Marine and Atmospheric Science
University of Miami
Coral Gables, Florida

ABSTRACT

A time series of the Loop Current in the
Gulf of Mexico, covering an annual cycle of
growth, spreading, and decay, has been ob-
tained in synchronization with ERTS. Com-
puter enhanced images, which are necessary
to extract useful oceanic information, show
that the current can be observed either by
color or sea state effects associated with
the cyclonic boundary. The color effect
relates to the spectral variations in the
optical properties of the water and its sus-
pended particles, and is studied by radi-
ative transfer theory. Significant oceanic
parameters identified are: the probability
of forward scattering, and the ratio of
scattering to total attenuation. Several
spectra of upwelling diffuse light are com-
puted as a function of the concentration of
particles and yellow substance. These
calculations compare favorably with experi-
mental measurements and show that the ratio
of channels method gives ambiguous inter-
pretative results. These results are used
to discuss features in images where surface
measurements were obtained and are extended
to tentative explanation in others.

/

Date: 25 January 1974

Reply to
Attn of: George A. Maul

Subject: Monthly Progress Report, T-4713-B

Refer to: RH1000-28M-48.03

To: Distribution List

This is the sixth report on project EREP 108, and it covers the month of December 1973.

The first attempt at a data take was performed on 3 December. The R/V VIRGINIA KEY sailed the afternoon of 2 December and was on station at the intersection of track 62 and the Florida Keys at sunrise the next day. The line began as soon as the zenith angle was 80°. Continuous measurements of chlorophyll-a and surface radiometric temperature were taken as well as close spaced samples of volume scattering function and BTs. At the first (and only) station spectral irradiance and plankton observations were made; the cloud cover was 75%. At the edge of the shelf the Gulf Stream peaked the seas up so that further stations were impossible. Further the cloud cover was increasing and the aircraft could obtain only two levels of the seven required. Therefore, at 1500Z the aircraft was radioed to abort the mission and both the ship and the aircraft headed back. (Later conversations with JSC revealed that the spacecraft would not have obtained the required data anyway). The ship was readied again for a pass on 8 December but that was cancelled by JSC.

On 11 December the P.I. gave an invited paper at the ERTS Symposium in Washington, D.C., entitled "Relationships Between ERTS Radiances and Gradients Across Oceanic Fronts", by George A. Maul and Howard R. Gordon (co-P.I.). Since this lays a significant foundation for the SKYLAB mission it is appended to this report.

Recipients of the financial report are marked by an asterisk on the attached distribution list.

INTRODUCTION

Remote sensing of the ocean in the visible region of the spectrum is being explored for a variety of reasons. Maximum insolation at 475 nm provides a natural energy source for passive sensors. A minimum in the attenuation coefficient for water may allow a passive measurement of some oceanic properties as a function of depth. Variations in the spectra of upwelling light at these wavelengths can be attributed to variations in pigment forming molecules such as in phytoplankton and to variations in the concentration of scattering particles such as suspended sediments. Strongly baroclinic currents in the subtropics and tropics can be detected by change in the optical properties across their boundaries when infrared techniques fail due to isothermal surface conditions. Patterns of man's activities in and on the ocean have near surface manifestations which change the nature of upwelling visible radiance.

The social significance of oceanic observations from a vehicle such as ERTS has recently been summarized by Maul (1974a). Discussions in the present paper are limited to a study of the dominant feature of the Gulf of Mexico circulation, that portion of the Gulf Stream System called the Loop Current. This intense current transports vast amounts of thermal and kinetic energy into the basin through the Yucatan Straits. Temporal and spatial variability in the flow (figure 1) was studied as part of the ground truth time-series which followed the anti-cyclonic turning from Yucatan to the Florida Straits. Some dynamical results were reported by Maul (1973a) and will not be discussed here. As a purely descriptive oceanographic study however, these data have significance in hurricane intensification studies such as by Leipper and Volgenau (1970); the investigation of the Florida east coast red tide (Murphy, *et al.*, 1973) used these ship tracks and a supporting ERTS image to document their arguments; the environmental impact of a recent accidental jettisoning of cyanide canisters following a ship collision in the Gulf of Mexico is being studied using these data (Corwin and Richardson, 1974). Continued reconnaissance of this current pattern is significant in our understanding of, and reaction to, the transport, which affects fishing industries, marine transportation, and public health.

ERTS OBSERVATIONS OF OCEANIC FRONTS

The location of the cyclonic boundary of the Loop Current was obtained by tracking the 22°C isotherm at 100 meters depth using expendable bathythermographs. The pathline of this

1

isotherm is of the order of 20 kilometers to the right
(facing downstream) of the surface frontal zone (Hansen and
Maul, 1970). This, coupled with ship observations of chloro-
phyll-a, surface temperature, volume scattering function, and
sea state, provides the baseline measurements to insure that
the interpretations to follow are well founded. Figure 2 is a
temperature-depth profile across the current along a suborbital
track during a satellite transit; surface observations are at
the top of the figure. This summarizes the general conditions
of increasing temperature and salinity and decreasing chloro-
phyll and scattering when crossing the boundary into the
current and serves to orient them to the indicator isotherm.
These observations confirm (Maul and Hansen, 1972) that
changes in all these properties occur simultaneously, allowing
an increase in confidence when a recognition decision is made
using several variables.

Diffuse reflectance from beneath the ocean, which is de-
fined as the ratio of upwelling to downwelling irradiance,
measured just above the surface, is rarely more than 0.05.
Reflectance from the ocean's surface, which is independent
of diffuse reflectance, can be comparable or even substantially
larger depending on sea state, and this has been shown by Maul
(1973b) to be a useful indicator of the current. Reflectance
from clouds and agricultural scenes is sometimes an order of
magnitude greater than from the ocean, even in the 500-600 nm
wavelength (λ) region. In order for the NASA Data Processing
Facility (NDPF) to produce an image for an average scene
radiance, the ocean signal is compressed into the lowest few
gray scales. This is clearly illustrated in figure 3 which is
a scanline plot across the boundary of the Loop Current from
the multispectral scanner. The large spikes in all four
channels (MSS 4 upper) are clouds; there seems at first glance
to be very little change in digital number (DN), which is pro-
portional to radiant intensity, as a function of the sample
number. However, careful examination shows that the average
value of the DN at samples greater than number 950 is slightly
larger than those before this point. It will be seen that
this marks the transition to higher radiances caused by in-
creased sea state in the current.

In order to graphically display this small change over a
two-dimensional region, computer enhancement is necessary.
Contrast stretching for the ocean scene is accomplished by
first studying the frequency distribution of DNs in a training
area on the image; the area is selected to be representative
of the ocean away from land and is large enough to be statisti-
cally significant. As seen from figure 3, such a histogram

2

would be strongly bimodal due to clouds. Selection of the upper (DN_u) and lower (DN_l) cutoff can be set at $\pm$ 2 standard deviations about the ocean mode; in this case $9 \leq DN \leq 13$ was used. It should be noted that each image will have different cutoff values and that the final image is quite sensitive to the range of DN chosen (Charnell *et al.*, 1973). The general expression for computing the stretch variable (ζ) is:

$$\zeta = M \left[\frac{DN_u - DN}{DN_u - DN_l} \right]^n \quad (\text{for } DN_l \leq DN \leq DN_u) \qquad (1)$$

where M is the maximum value allowed by the output device, and n is an arbitrary integer exponent. Equation 1 produces a negative of the input digital image; positive whole integers n, further stretch the low radiance values encountered in the ocean. The graphic result of using equation 1 on the data from which figure 3 was taken is given in figure 4.

Figure 4 is a negative print of an area due north of the Yucatan Straits using MSS 5 data. Computer enhancement in this iamge uses only five gray scales of the 128 levels available; all values below DN_l are set to 127 and all above DN_u are set to 0. The boundary between the resident Gulf waters (left) and the current (right) is seen as a transition from light to dark tones respectively. Since the radiance levels in the ocean are so low, the oceanographer *must* resort to computer enhancement as this example shows.

Figure 5 is another enhancement of the Loop Current boundary using MSS 5 where $7 \leq DN \leq 15$ and n = 2. In this negative image of the western Florida Keys, water from Florida Bay extends into the Florida Straits and is entrained by the Loop Current. The current boundary in both figures 4 and 5 was delineated by surface vessel tracks during the day of the satellite transit. Notice that the current is darker in tone (higher in radiance) in figure 5. This is caused by the dominance of surface reflection due to higher sea state in the current in figure 4, as compared to higher reflectance due to particles in the Florida Bay water in figure 5.

SOME THEORETICAL CONSIDERATIONS

At this point it is useful to consider in detail the processes contributing to the radiance spectrum $N(\lambda)$ at the position of the satellite. Solar radiation incident at the top of the atmosphere is absorbed and scattered in the atmosphere. Some radiation is scattered back into space without striking the

3

ocean contributing a radiance $N_s(\lambda)$ at the satellite. The rest (which is not absorbed) will interact with the ocean. This interaction can yield upwelling radiance above the ocean in three ways: 1) specular reflection from the surface; 2) diffuse reflection from foam (bubbles) on or just beneath the ocean surface; and 3) the diffuse reflection from water molecules and suspended particles in the water. Of these the first two phenomena are closely related in that they depend on the sea state, while the third source of radiance is essentially independent of sea state. The specular reflectance from the rough ocean surface can be computed by the methods of Cox and Munk (1954) in terms of the wind speed and incident radiance distribution. The diffuse reflectance from white caps can be approximately accounted for by assuming they are "white", Lambertian, and have an albedo of 1 so that they contribute uniform upwelling radiance just above the surface given by

$$ H_0(\lambda) \frac{f}{\pi} $$

where f is the fraction of the scene covered by the white caps and $H_0(\lambda)$ the irradiance incident on the sea surface. The third source of radiance, that from beneath the surface, is the most difficult to compute and will be discussed in detail below. We can write the radiance at the satellite as

$$ N(\lambda) = N_S(\lambda) + \gamma(\lambda)N_{SS}(\lambda) + \alpha(\lambda)\, N_d(\lambda) \tag{2} $$

where $N_{ss}(\lambda)$ is the contribution at the surface due to reflection from the surface and white caps, N_d is the diffuse radiance just above the surface due to photons that have penetrated the ocean, $\alpha(\lambda)$ and $\gamma(\lambda)$ are atmospheric transmittance factors for N_d and N_{ss}. $\alpha(\lambda)$ and $\gamma(\lambda)$ are in general not equal since the radiance distribution (variation with angle) of N_{ss} and N_d are different. It is possible for photons to be reflected from the surface, backscatter from the atmosphere into the ocean, and scatter back into the atmosphere. Photons which do this we consider to be a part of N_d. It should be stressed at this point that $N_d(\lambda)$ in the above equation is the *only* source of radiance that contains information about conditions beneath the sea surface such as the concentration and composition of suspended particles and dissolved organic material. A thorough understanding of the dependence of $N_d(\lambda)$ on the basic optical properties of the water and its constituents is required in order to obtain *quantitative* information about the constituents of the ocean from measurements of $N_d(\lambda)$. The remainder of this section is devoted to relating $N_d(\lambda)$ to these optical properties.

4

We shall assume that the radiance distribution incident on the sea surface is given, and that the radiance is transmitted from the ocean to the satellite in a known manner given by $\alpha(\lambda)$ and $\gamma(\lambda)$ in equation 2. This reduces the problem to that of taking a known downwelling radiance distribution just above the sea surface, and computing the distribution (just above the surface) of the upwelling radiance. As mentioned above, radiant energy interacting with the ocean can be absorbed by water, suspended particles, and dissolved organic material commonly called yellow substance with absorption coefficients a_w, a_p, a_y respectively and scattered by the water and particles with scattering coefficients b_w and b_p (scattering by the yellow substance appears to be negligible). The total attenuation coefficient, c, for these interactions is given by

$$c = c_w + c_p + c_y \tag{3}$$

where

$$c_w = a_w + b_w,$$
$$c_p = a_p + b_p, \tag{4}$$
$$c_y = a_y$$

are the beam attenuation coefficients of the water, particles, and yellow substance. The scattering is further characterized by the phase function, $P(\theta)$, which relates to the intensity of radiation, $dJ(\theta)$, singly scattered from a small sample volume, dv, when illuminated by an incidence irradiance, H_o, through

$$P(\theta) = \frac{dJ(\theta)}{(H_o dv)b}$$

$$2\pi \int_0^\pi P(\theta)\sin\theta\, d\theta = 1 . \tag{5}$$

The total phase function for water and particle scattering is

5

$$P(\theta) = \frac{(b_W P_W(\theta) + b_p P_p(\theta))}{(b_W + b_p)}$$

where P_W and P_b are the phase functions due to water only and particles only respectively. It is convenient to further define the forward (F) and backward (B) single scattering probabilities by

$$B \equiv 1 - F$$

$$F \equiv 2\pi \int_0^{\pi/2} P(\theta) \sin\theta \, d\theta \qquad (6)$$

and the single scattering albedo by

$$\omega_0 \equiv \frac{b}{c} \qquad (7)$$

Hence it is clear that

$$B = \frac{(b_p B_p + b_W B_W)}{(b_p + b_W)} \, , \qquad (8)$$

$$\omega_0 = \frac{(b_W + b_p)}{(a_W + a_p + a_y + b_p + b_W)} \, , \qquad (9)$$

and in general, $\qquad 0 \leq \omega_0 \leq 1 \, .$

It should be noted that *all* of the above quantities depend on wavelength (λ). The transfer of radiation in the ocean is governed by the radiative transfer equation which has been discussed in detail by Chandrasekhar (1960) and Preisendorfer (1965). Gordon and Brown (1973) have computed the diffuse reflectance (upwelling irradiance/incident irradiance) just above a flat *homogenous* ocean as a function of its optical properties by a Monte Carlo technique. Using a combination of the parameters which arise naturally from the quasi-single scattering model (Gordon 1973), Gordon, Brown and Jacobs (in preparation) show that the diffuse reflectance (R_d) can be written

$$R_d = 0.179x + 0.0510x^2 + 0.1710x^3 \qquad (10)$$

6

where
$$X \equiv \frac{B\omega_0}{(1-\omega_0 F)} \quad .$$

R_d is to first order independent of the distribution of the incident irradiance. It should be emphasized that the above equation does *not* include the irradiance specularly reflected from the sea surface or white caps, i.e. R_d is the contribution to the reflectance from photons which penetrate the surface and are multiple scattered back into the atmosphere. Preliminary computations (Gordon and Brown unpublished) indicate equation 9 is also valid for a moderately rough surface. The radiance distribution above the sea surface (due to photons scattered out of the ocean) is only weakly dependent on ω_0, and thus the radiance at any viewing angle will in first order vary with ω_0, and B in the same fashion as R_d. Hence, it is sufficient to study the influence of the optical properties of the ocean on R_d alone.

Equation 9 shows that the important oceanic parameters are ω_0 and B, and so the observed reflectance spectrum, $R_d(\lambda)$, can be explained entirely through a knowledge of $\omega_0(\lambda)$ and $B(\lambda)$. Conversely under *optimum* conditions, only $\omega_0(\lambda)$ or $B(\lambda)$ can be deduced from R_d and then only if *one* of these quantities is already known. The situation appears quite depressing when it is realized that $\omega_0(\lambda)$ is only imperfectly known even for pure water and to our knowledge there are no measurements of $B_p(\lambda)$ and $\omega_0(\lambda)$ for various kinds of suspended particles. Hence at the present time it is difficult to interpret $\omega_0(\lambda)$ and $B(\lambda)$ even if both could be extracted from $R_d(\lambda)$ measurements. This underscores the necessity of laboratory experimentation to determine these optical properties for various ocean constituents such as marine phytoplankton, and suspended mineral particles, for adequate interpretation of oceanic "color". If the optical properties of the constituents are known, then it is theoretically possible to determine their concentrations through observations of $R_d(\lambda)$ as is discussed in several examples below.

We shall now examine a particularly simple problem of interpretation, that of determining the concentration of suspended material in the absence and presence of yellow substance. The particles are assumed to be nonabsorbing, and their scattering coefficient is assumed to be independent of wavelength [cases where $b_p = (const.) \lambda^{-n}$ with $n \leq 1$ have also been investigated and yield results not dramatically different from the $n = 0$ case]. These calculations will *not* apply at all to locations with particles containing absorbing pigments such as phytoplankton in the water, since Mueller (1973) and Gordon (1974) have shown that scattering from such particles varies *strongly* with wavelength near the pigment absorption bands.

7

In order to use equation 10, $B(\lambda)$ and $\omega_o(\lambda)$ in equations 8 and 9 must be determined. We shall follow Tyler, Smith and Wilson (1972) and use for b_w and B_w values experimentally computed for sea water continuously filtered for 18 hours (Petzold 1972), rather than theoretical computations of these quantities for pure water. We do not feel comfortable with this, however, on the above basis they have estimated the absorption spectrum of "clear natural water", and since we use their $a_w(\lambda)$ spectrum this assumption is essential for consistency. It is thus assumed that $B_w = 0.1462$ and $b_w = 0.008 m^{-1}$ at 550 nm, so

$$b_w = 0.008 \left[\frac{550}{\lambda}\right]^4 m^{-1}$$

To find B_p, Petzold's measurements of $P(\theta)$ from the Tongue of the Ocean (TOTO), San Diego Harbor (SDH), and Off Shore California (OSC) at 530 nm have been used. Assuming the above for B_w and b_w, the contribution from water is subtracted yielding the B_p values listed in Table 1 (ω_o is given in the parenthesis and ω_o for filtered sea water at this wavelength is 0.136).

TABLE 1

Derived Values of B_p for the Indicated Locations

TOTO	SDH	OSC
0.0165 (.59)	0.0186 (.82)	0.00966 (.59)
0.0158 (.25)	0.0194 (.83)	0.00836 (.55)
0.0130 (.26)	0.0169 (.91)	0.00836 (.55)

From Table 1 it is clear that B_p not only varies considerably from one location to another, but also varies considerably for a single region. This is unfortunate in that for small ω_o, R_d is directly proportional to $\omega_o B$ and ω_o and B are then *equally* important in determining R_d for these cases. We shall assume that Table 1 gives the range of variation of B_p to be expected in natural waters, however this is probably not the case. Furthermore we will assume B_p (and B_w) is independent of wavelength.

Since a_p is taken to be zero, and the $a_w(\lambda)$ estimate of Tyler, Smith and Wilson is to be used, only $a_y(\lambda)$ remains to

be considered. This is taken from Jerlov (1968, Page 56) and
is parameterized by .

$$a_y(\lambda) = a_y e^{0.0145(550-\lambda)}$$

where λ is in nm. Reasonably high concentrations of yellow
substances in the open ocean have $a_y \simeq 5 \times 10^{-3} m^{-1}$ (i.e.,
near Galapagos Islands) however, a_y can be much larger in
coastal regions.

Using the above and equation 10, we have computed $R_d(\lambda)$
called Reflectance $(0,-)$ in the figures, as a function of
b_p/b_w (proportional to the concentration of suspended par-
ticles) for various values of B_p and a_y. The results are
given in figures 6 through 10.

Figure 6 shows the R_d for $\lambda = 550$ nm as a function of
b_p/b_w and B_p. The linearity of R_d with b_p/b_w is to be noted.
These results clearly demonstrate the importance in knowing
B_p for a quantitative determination of the particle concen-
tration from R_d (which is measured at the *sea surface*).
Figure 7 shows spectra of R_d again for various values of
b_p/b_w but now with $B_p = 0.0165$. These spectra have the same
general shape as those observed by Tyler and Smith (1970)
just beneath the surface in Crater Lake, but are not in
quantitative agreement even when the loss due to transmittance
through the water surface is considered. Basically the
difference is that quantitative agreement requires too large
a value of b_p/b_w. This could be due to the value of B_p used,
the fact B_p is assumed to be independent of wavelength, or
inaccuracies in their estimated $a_w(\lambda)$ on which the present
calculations are based. In any event the computations can be
used as a guide for examining ERTS related data. Figure 8
shows the influence of yellow substance on the reflectance
for the case with $b_p/b_w = 128$ and $B_p = 0.0165$. The major
influence of the yellow substance is to depress the blue
region of the reflectance spectrum. All of these results are
summarized in figures 9 and 10, where the reflectances have
been integrated over the ERTS MSS channels 4 (figure 9) and
5 (figure 10) for various B_p and a_y as a function of b_p/b_w.
It is seen that the yellow substance influences the reflec-
tance in MSS 4 only at very high concentrations (for the open
ocean) and essentially plays no role in the MSS 5 reflectance.
Therefore, for suspended particle concentrations, it appears
that MSS 5 is best with MSS 4 only slightly degraded by the
dissolved organic materials. It should be emphasized again
that the above discussion refers only to the case of no
phytoplankton (chlorophyll)!

9

We now turn to the problem of estimating b_p/b_w or some related quantity from satellite observations. Since the above calculations are only for the case of negligible phytoplankton (chlorophyll) concentrations we must find criteria from which to choose which ERTS channels will satisfy this constraint. Also unless only MSS 5 is used we expect yellow substances to be important especially in coastal regions where river runoff, etc., may be considerable. Furthermore there is the additional problem that the reflectance depends on B_p which is also unknown, as will as b_p/b_w. We have developed a method which partially overcomes some of these problems. Considering the radiances observed in MSS 4 and 5, we have approximately

$$N_4 = \alpha_4 N_{d_4} + \gamma_4 N_{ss_4} + N_{s_4}$$

$$N_5 = \alpha_5 N_{d_5} + \gamma_5 N_{ss_5} + N_{s_5} \tag{11}$$

where α_i and γ_i ($i = 4, 5$) are the fractions of N_{d_i} and N_{ss_i}

(measured at the sea surface) that reach the sensor. It is assumed that α_i and γ_i are constant over an ERTS Frame (if they vary in a known way, their influence is easily accounted for and will not be discussed further). Now from the theory

$$N_{d_4} = k_4 \frac{b_p}{b_w}$$

$$N_{d_5} = k_5 \frac{b_p}{b_w} \tag{12}$$

where k_4 and k_5 are essentially independent of b_p/b_w, but depend directly on B_p. Taking the horizontal gradient, ∇_H, of equation 11 using equation 12 we find

$$\nabla_H N_i = k_i \alpha_i \nabla_H \left(\frac{b_p}{b_w} \right) + \gamma_i \nabla_H N_{ss_i} \tag{13}$$

since N_{s_i} is nearly constant over a frame ($\nabla N_{s_i} = 0$). The last term in equation 13, $\nabla_H N_{ss_i}$, is the horizontal gradient of the reflected radiance from the sea surface. This is nearly zero everywhere except where the sea state changes dramatically with horizontal distance (for example in figure 4). Nearly everywhere on the frame then, $\nabla_H N_{ss_i} = 0$, so

$$\frac{\nabla_H N_4}{\nabla_H N_5} = \frac{k_4 \alpha_4}{k_5 \alpha_5} \tag{14}$$

10

Again α_4/α_5 is constant (or slowly varying) over the scene;
so almost everywhere in the frame, variations in $\nabla_H N_4 / \nabla_H N_5$
are the result of variations in k_4/k_5. Now if
B_p is constant, or if the "mean" B_p is constant in each
wavelength band, this would imply that essentially only the
concentration of scattering particles varies over the frame,
i.e. not the nature of particles or their size distribution.
In this case, k_4/k_5 would be constant. Hence essentially
k_4/k_5 will vary, if the nature or size distribution of the
particles varies over the frame (B_p changes), or if the
yellow substance concentration varies considerably over the
frame, which would force k_4 to vary independently of k_5.
Thus if we find

$$\frac{\nabla_H N_4}{\nabla_H N_5} = Const$$

(15)

it is reasonable to expect that *only* the particle concentration
changes over the frame. In this case

$$\nabla_H N_4 \text{ or } \nabla_H N_5 \sim \nabla_H \text{ (particle concentration)}$$

(16)

Note here that these relations should also apply to scenes
containing phytoplankton if they are the dominant scatterers;
but for mixtures of phytoplankton and suspended white particles,
one would expect equation 15 to be violated over a scene if the
relative concentrations vary drastically. To reiterate, if 15
holds, probably only the particle concentration varies over the
frame, and 16 can be used to measure the gradient of its con-
centration. Since B_p is unknown, the actual concentration is in-
determinate without ground truth to better than a factor of two,
since this is the assumed uncertainty in B_p. Several examples of
the use of the above ideas for analysis of ERTS data are pre-
sented below.

DISCUSSION

Equation 16 was applied to MSS 4 and MSS 5 data in
figure 11. This computer enhanced negative image of the
Cape Hatteras region shows what appears to be large gradients
in suspended sediment. The Gulf Stream apparently has
entrained particles from Rayleigh Bay and is carrying them
out to sea. Along the scanline shown we have computed

$$\frac{\partial}{\partial x}\left[N_4\right] = g\frac{\partial}{\partial x}\left[N_5\right] + h$$

(17)

11

properties of the individual components with wavelength is known.

As an example of this, the spectra given in figure 12 were integrated over the MSS 4, MSS 5, and MSS 6 filter functions. A series of numerical tests were then made of ratios, differences, and sums to see if the three water types could be distinguished at the sea surface. It was quite easy to distinguish on the basis of such calculations between the Gulf Stream waters and the coastal waters, and between the coastal waters and the plankton bloom; however it was *not* possible to distinguish between the Gulf Stream and the plankton bloom. This suggests, as the theory implies, that for these data the ratio test (MSS 4/MSS 5) is not likely to be successful in specifying the chlorophyll-a concentration. Further, since the sea surface component, N_{ss}, (λ), spectrally alters N (λ), numerical tests (ratios, differences *etc*.) are *invalid* indicators of oceanic properties.

Probably the most efficient method of determining the concentration of the constitutents in the ocean will be to compare theoretical and experimental spectra, adjusting the constitutent concentrations in the theoretical spectra until agreement is found. This of course requires a basic under-standing of the optical properties of the constitutents which can be derived only from careful *in situ* and laboratory experi-ments. It seems that at the present time much energy and money is being expended to try and use optical methods to locate and study materials with nearly unknown optical pro-perties suspended or dissolved in a medium with only poorly known optical properties. This must be overcome before significant progress can be made.

A final interpretation of oceanic observations from ERTS is given in figure 13 which is a computer enhanced MSS 6 negative image of southeastern Florida. The dark lineation parallelling the coast in the upper portion of the image is a zone of high reflection caused by locally increased N_{ss} along the edge of the Florida Current. The increase in surface reflectance is probably caused by surface wave interaction with the cyclonic boundary and is not bottom influence. This further explains the edge effect and supports the discussion on the local dependence of $\nabla_H N$ on $\nabla_H N_{ss}$ only given above. Another example of the dominance of N_{ss} is the bright slick areas (low N) off the Virginia Key sewer treatment plant. This is probably caused by the dampening of the glitter causing capillary waves in the oil film associated with the organic slick. The slick, which has drifted south past the popular Key Biscayne beaches, offers an explanation of the narrow lineation off shore in the Florida Straits: a passing oil tanker heading south which is pumping her bilges would cause

where the least squares values for g=0.38 and h=0.00, and the
linear correlation coefficient, r, is 0.66. The coefficient of
determination, r^2, which is the ratio of the explained varia-
tion from the mean (by the least squares line) to the total
variation, is 44%. Physically this means that this image *may*
not be useful for determining particle concentrations because
B_p, ω_o (i.e. a_y), or b_p/b_w may be changing. The extent to which
this holds true in natural waters is unknown; this will be
extensively tested in the New York Bight area where turbidity
measurements are being made by NOAA vessels concurrent with
ERTS transits.

The data of figures 7 and 8 can be compared to measure-
ments of upwelling irradiance. Data given in figure 12 were
observed using a ¼-meter Ebert spectroradiometer from 3 meters
above the surface; these observations were made during the
time frame of figure 5 and represent the water types shown in
that image. All spectra were carefully selected to represent
the same downwelling irradiance, sea state, sun angle, cloud
cover, and absence of bottom influence. Specular reflection
due to waves were minimized by preselecting ten spectra with
similar shapes. After digitizing the records, averages and
standard deviations (σ) were computed at each wavelength; if
values exceeded the average by 1σ, they were rejected and a
new mean computed. Absolute values of the spectra are traced
to NBS through the 2-meter integrating sphere at NASA's
Goddard Space Flight Center.

As the chlorophyll-a concentration increases, the spectral
peak shifts to longer wavelengths in similarity with the com-
puted data in figure 8. This is not to say that the chloro-
phyll-a and the yellow substance produce *quantitatively* similar
results; in general they will not. What it does imply is that
the broad absorption bands in pigments such as chlorophyll and
yellow substance at shorter wavelengths (<600 nm) produce
qualitatively similar effects in the spectra. When other fac-
tors are equal, increasing the concentration of pigments will
cause a decrease in the radiance in MSS 4 only. In nature
however, such as in a plankton bloom or in a river plume,
increased amounts of chlorophyll are normally accompanied by
increased particle concentrations (organisms which contain
the chlorophyll) as well as yellow substances (decay products
of the plankton), and increased amounts of "white" suspended
particles in the river plume case. The radiances in MSS 4
and 5 will in these cases vary in a manner which will depend
again on the relative concentration of the constitutents, and
since a and b vary almost independently, the reflectance
signature, which depends on $\omega_o(\lambda)$ and $B(\lambda)$ is not unique and
can be unraveled only when the variation of the optical

13

a similar feature on the image. Thus ERTS could be useful in patrolling coastal waters for such illegal acts which affect the nearshore water quality.

CONCLUSIONS

The spectral properties of the oceanic front associated with the Loop Current have been studied by ship and satellite observations and by radiative transfer theory. It is seen that computer enhancement is required to extract useful information from the ERTS data for the ocean scene. The current boundary can be detected by changes in the surface reflectance, N_{ss}, as well as the diffuse reflectance, N_d, from below the surface; N_d however is dependent on both B and ω_o, and thus the spectral interpretation of ocean color *requires* surface truth measurements for meaningful results. Particle concentrations, which can delineate currents, can be estimated in MSS 5 if the ratio $\tau_H N_4 / \tau_H N_5$ is reasonably constant over a scene. MSS 4 is strongly influenced by yellow substance, and particle estimation based on these data are invalid in many coastal zones. Water mass identification using ratios or differences of MSS 4, 5, and 6 data have no validity in either theory or observation in the Gulf of Mexico. Finally, it must be emphasized that the spectrum of upwelling radiance just above the surface is a function of both N_d and N_{ss} and that N_{ss} frequently dominates.
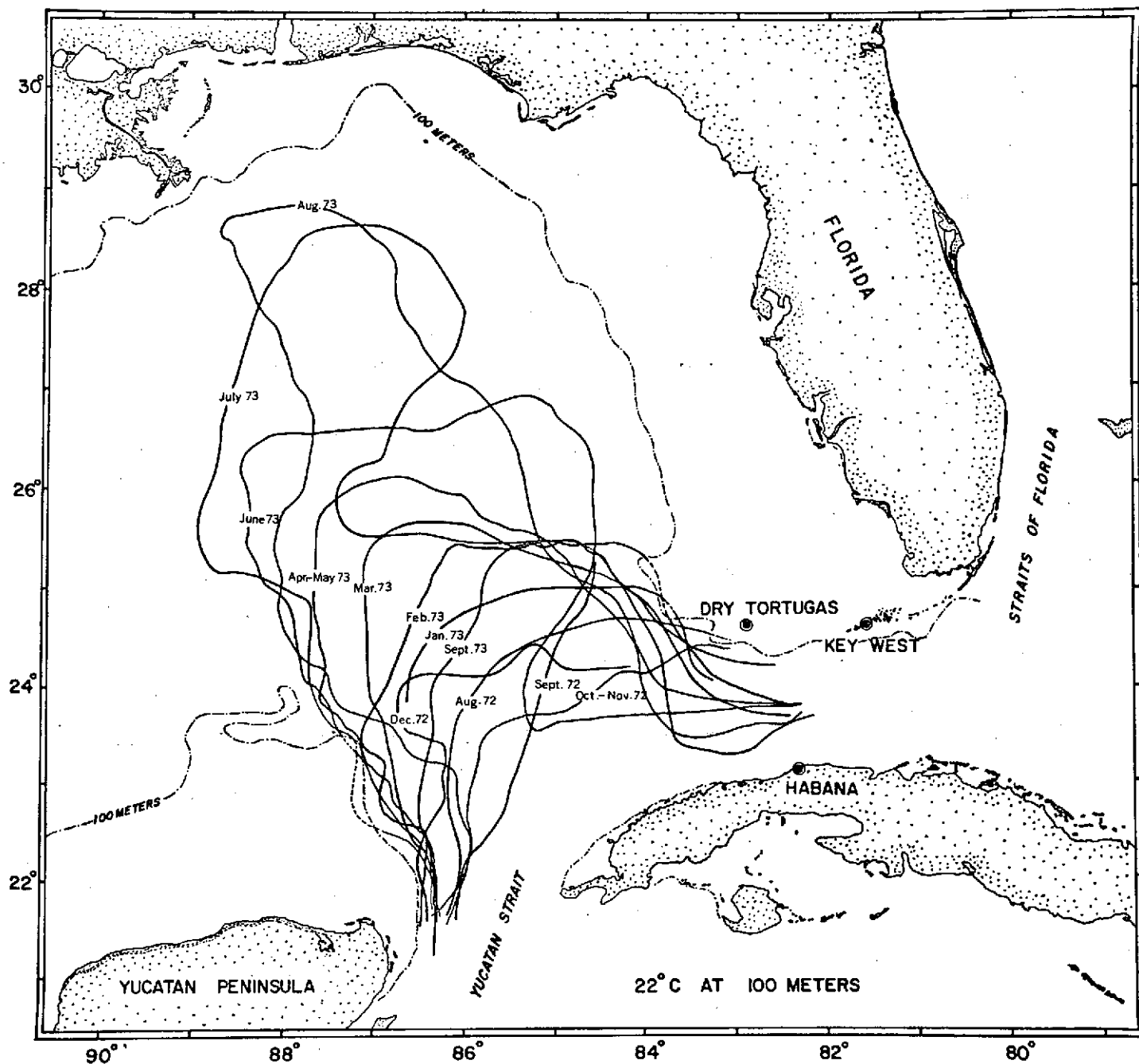

ACKNOWLEDGEMENTS

Figure 1. Time series of the Loop Current in the Gulf of Mexico, August 1972-
September 1973. The pathlines are the location of the 22°C isotherm
at 100 meters depth. Each cruise was synchronized with ERTS passes
over the area every 36 days. The indicator isotherm was located by
expendable bathythermographs from a surface vessel; this isotherm is
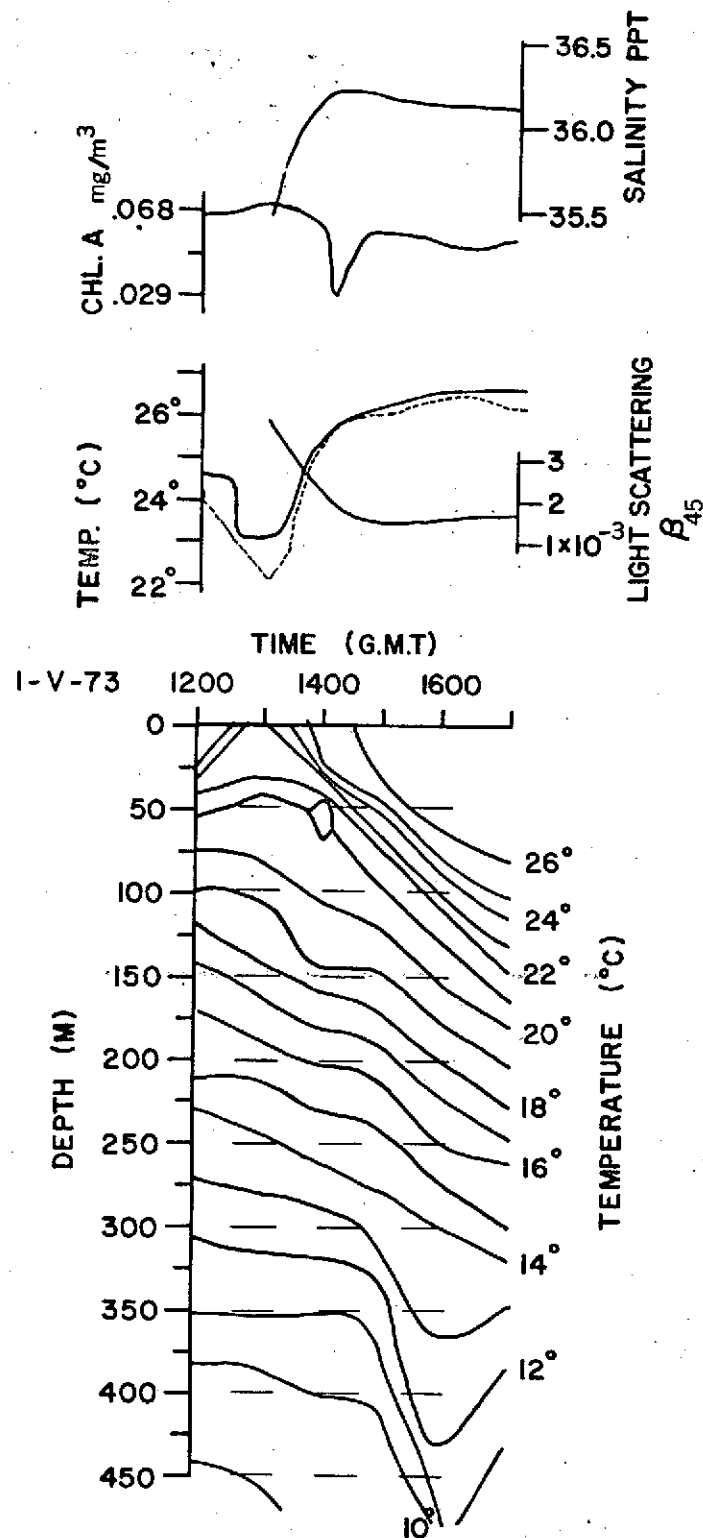approximately 20 kilometers to the right of the cyclonic edge facing
downstream.

15

Figure 2. Cross section of the Loop Current taken by ship along a suborbital track on the day of ERTS transit. Section shows typical increase in salinity and temperature (dashed-radiometric, solid-bucket) when crossing into the current. Similarly chlorophyll-a and volume scattering function at 45° (436nm light) decrease. The temperature-depth section shows the relation between the 22°C at 100 meters and the surface frontal zone (at ca. 1330 GMT). Horizontal scale is 5 hours travel time at 9.8 knots or 90 kilometers.
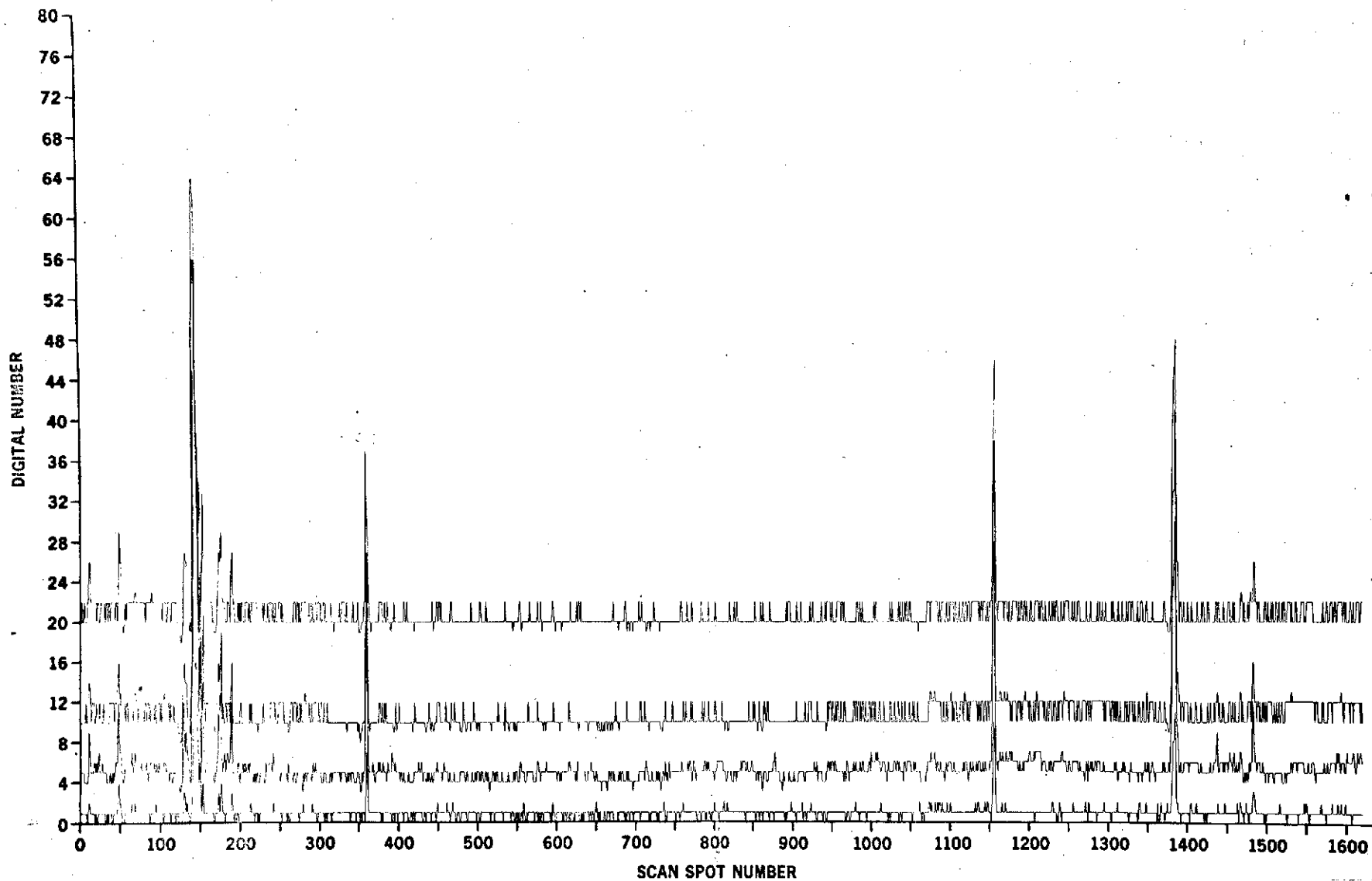
16

Figure 3. ERTS scanline plot across the Loop Current front. Top scanline is MSS 4, next MSS 5, MSS 6, and MSS 7 on the bottom. The large energy spikes are clouds. At scan spot number 950 there is an increase in the average value of the digital number of 1 or 2; this marks the cyclonic edge of the current.
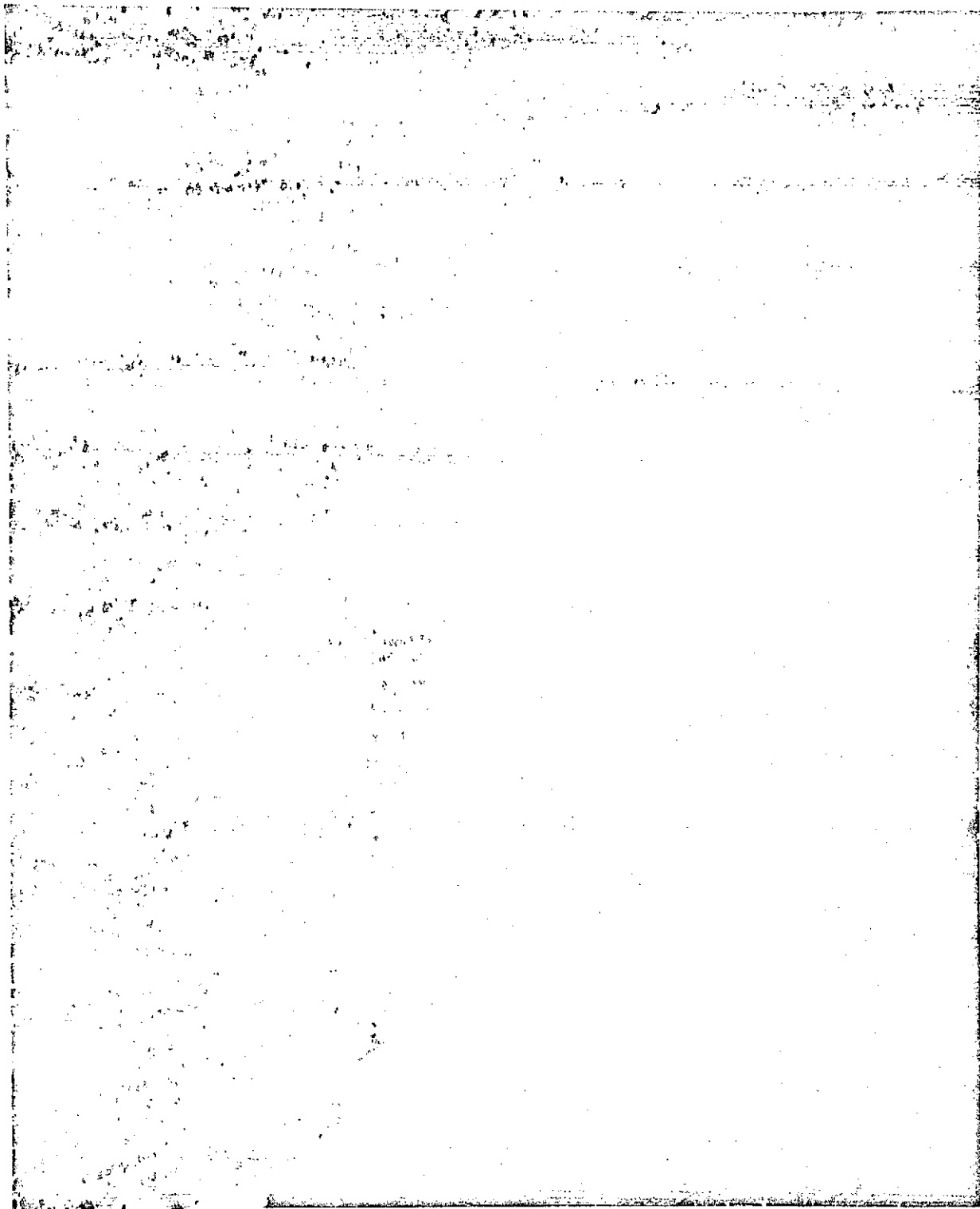
17

Figure 4. Negative print of computer enhanced (9<DN≤13; n = 1) MSS 5 image of the cyclonic boundary of the Gulf Loop Current. Surface vessel track confirmed the location of the current to be the darker shade (higher radiance) region on the right hand side of the image (ERTS ID 1065-15411). Scanline plot in Fig. 4 horizontally passes through the middle of the scene. Horizontal distance across the image is 90 kilometers.
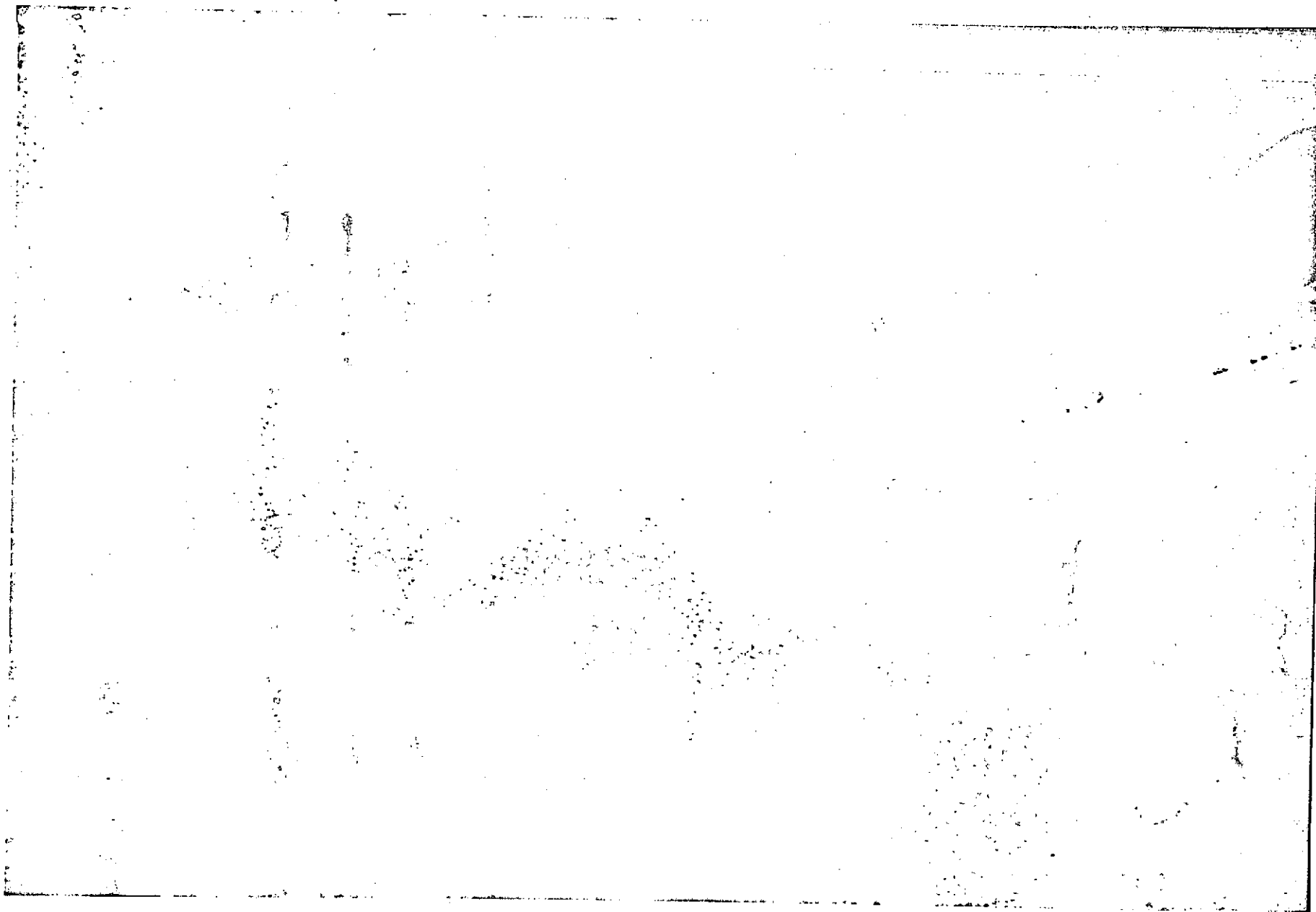
Figure 5. Negative print of computer enhanced (7<DN<15; n = 2) MSS 5 image of Marquesa Key and Key West (ERTS ID 1099-15293). Change in radiance southwest of Marquesa from dark to light marks the ship-located boundary between the higher intensity Florida Bay water and the lower intensity Gulf Stream. Bottom depth is in excess of 100 meters and thus does not contribute to the radiance. Horizontal distance across the image is 135 kilometers.
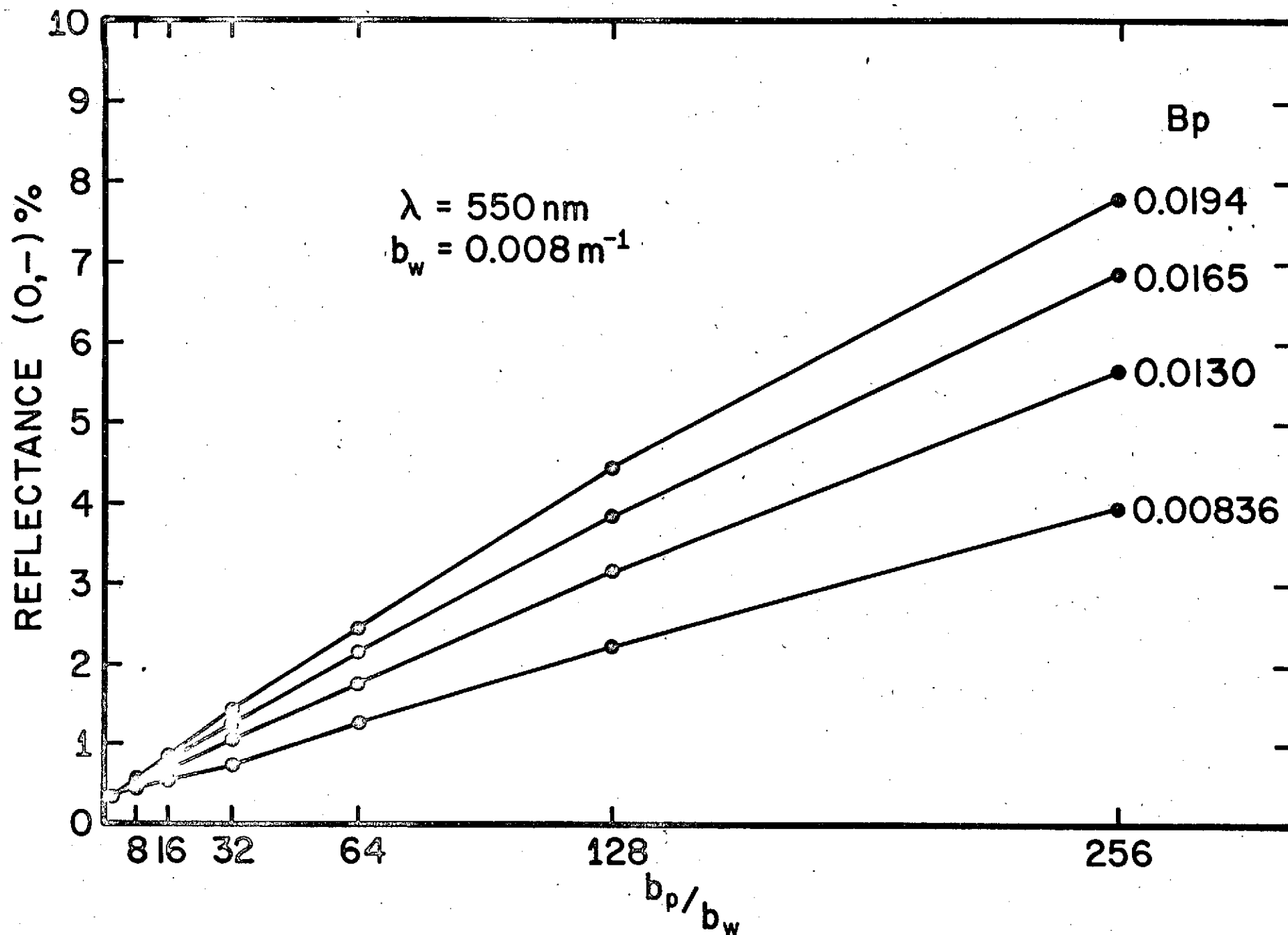
Figure 6. Computed reflectance in percent at the sea surface as a function of the ratio of the particle scattering coefficient to the water (only) scattering coefficient for 550nm. The value of the fraction of backscattered light due to particles (B_p) for each curve is given on the right hand side.
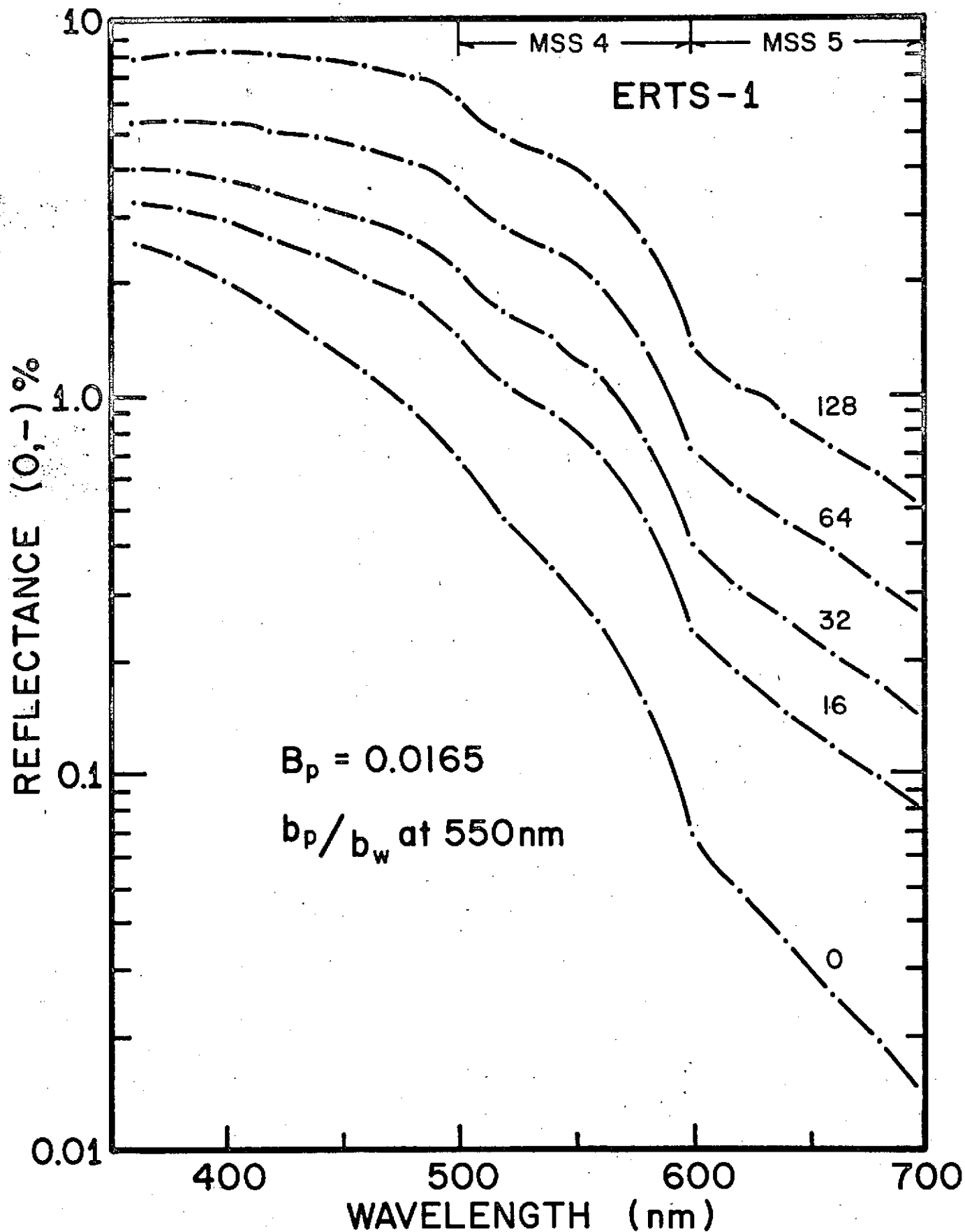
Figure 7. Computed reflectance in percent at the sea surface as a function of wavelength for various values of the ratio of the particle scattering coefficient to the water scattering coefficient. Note the wavelength dependence in these spectra of changing the particle concentration only.
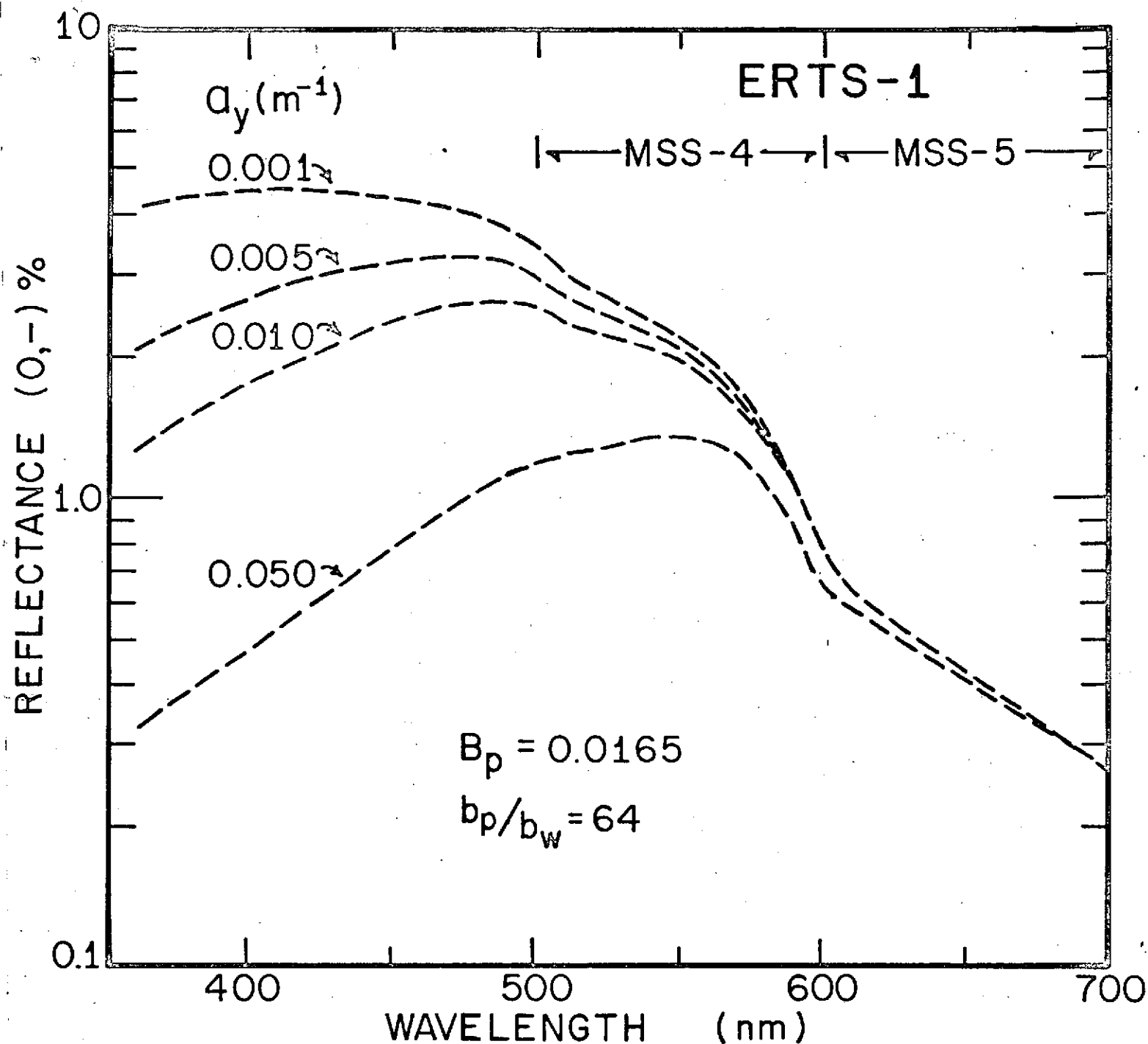
Figure 8.   Computed reflectance spectra, in percent, at the sea surface. The ratio of the particle to water scattering coefficients (b_p/b_w) and the fraction of backscattered light are 128 and 0.0165 respectively. Values of the absorption coefficient due to yellow substance (a_y) are listed on the left hand side. Note the shift of the spectral peak to longer wavelengths with increasing a_y.
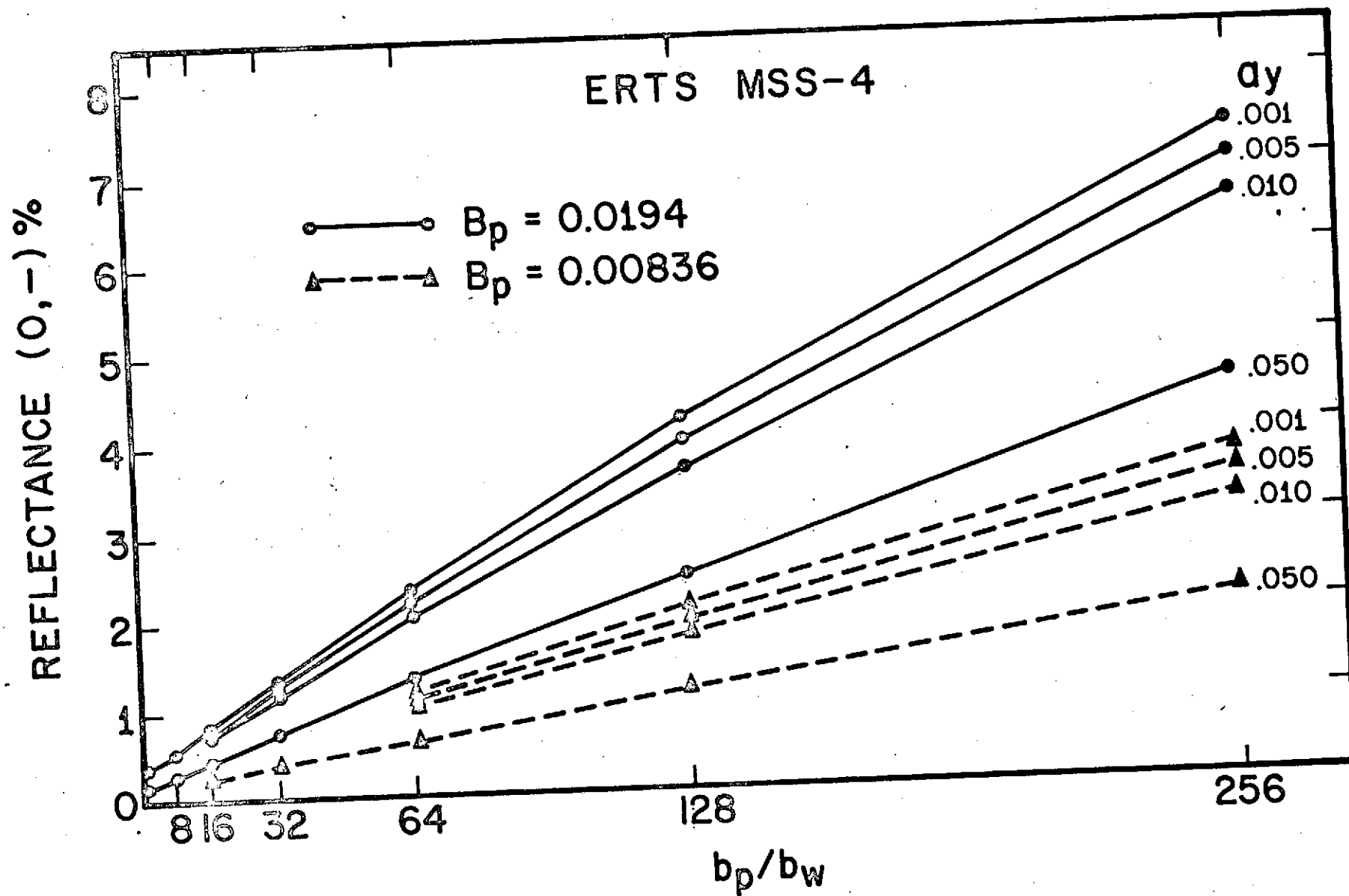
22

Figure 9. Computed reflectance in percent at the sea surface as a function of the ratio of the particle to the water scattering coefficients integrated over the spectral response of the MSS 4 filter (0.5-0.6μm). Values of the absorption coefficient due to yellow substance (a_y) are listed along the right hand side. Note the linearity depends on both a_y and the fraction of backscattered light, (B_p).
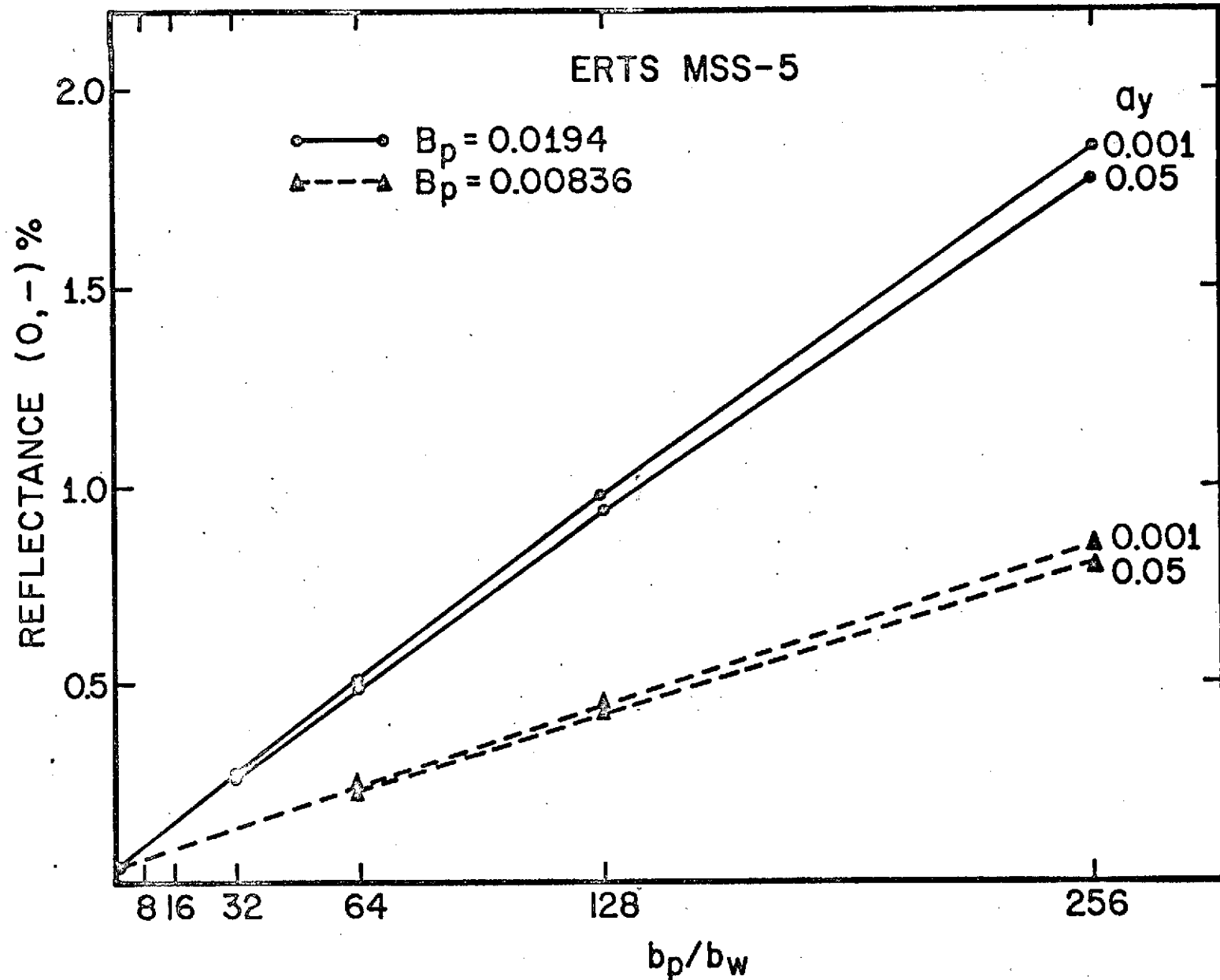
Figure 10. Computed reflectance at the sea surface, in percent, as a function of the particle to water scattering coefficient ratio, integrated over the response function of the MSS 5 filter (0.6-0.7μm). Values of the absorption coefficient due to yellow substance (a_y) are listed along the right hand side. Note the linearity is not strongly dependent on a_y but only on the fraction of backscattered light, B_p.
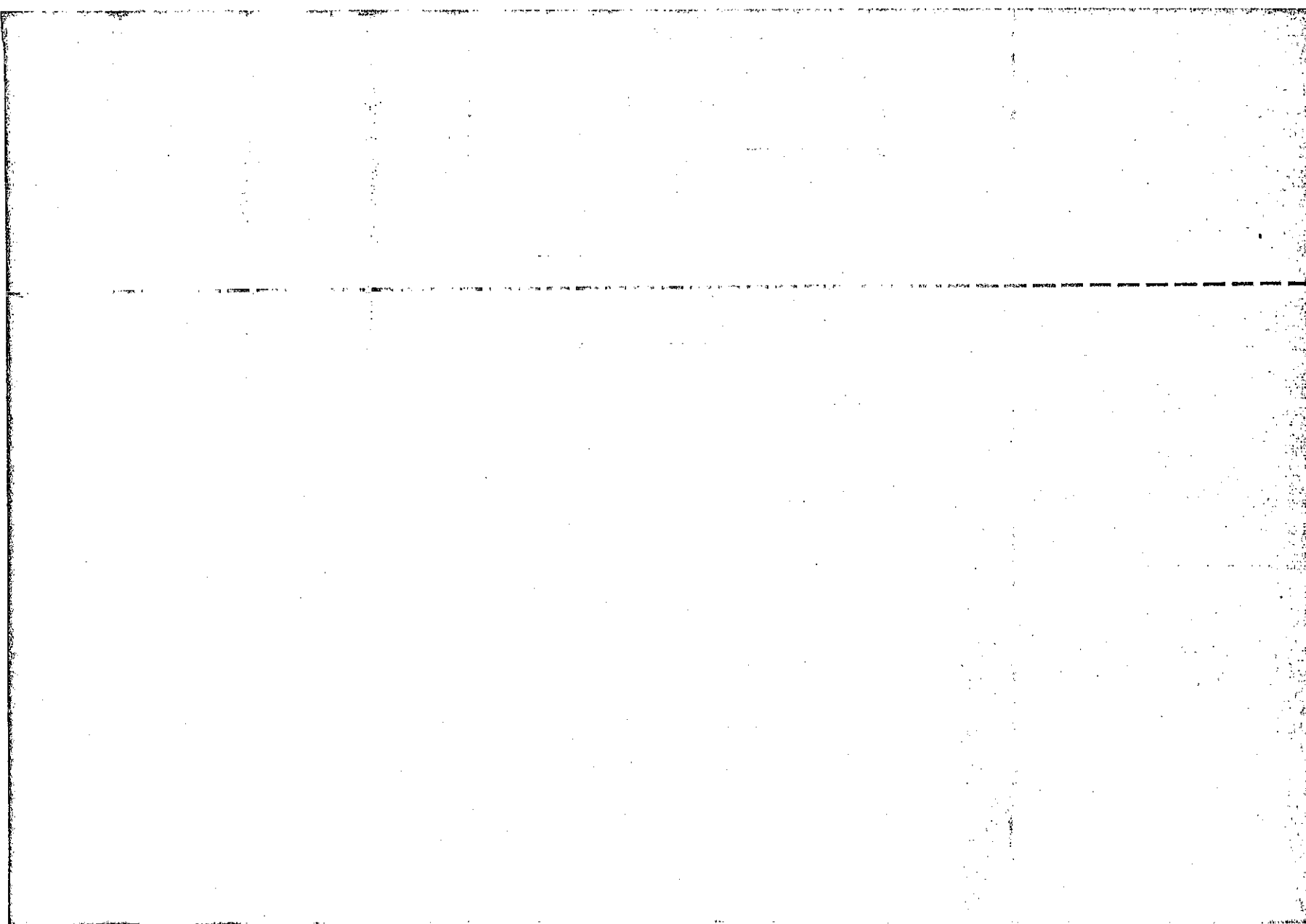
Figure 11. Contrast stretched (4<DN<12; n = 2) negative image of the ocean area offshore of Cape Hatteras (ERTS ID 1132-15042). The Gulf Stream can be seen as the bright area to the south of the entrained sediment from the coastal estuaries. The least squares fit of eq. (17) was done along a scanline north of the Cape and extending from nearshore, through the suspended sediment and into the current. Extensions of this plume were observed for 150 kilometers further east on other ERTS images. Horizontal distance across the image is 135 kilometers.

UPWELLING IRRADIANCE $\left[\text{ m W cm}^{-2}\,\mu\text{m}^{-1}\right]$

10

PLANKTON Chl-a: 4.13 mg m^{-3}
BLOOM $\quad \beta_{45}$: $\quad$ 9.2 x 10^{-3}m^{-1}

GULF STREAM

Chl-a: 0.13 mg m^{-3}

β_{45}: $\quad$ 1.7 x 10^{-3}m^{-1}

5

COASTAL
Chl-a: 0.28 mg m^{-3}
β_{45}: $\quad$ 6.7 x 10^{-3}m^{-1}

0

.4 $\quad$ .5 $\quad$ .6 $\quad$ .7 $\quad$ .8 $\quad$ .9
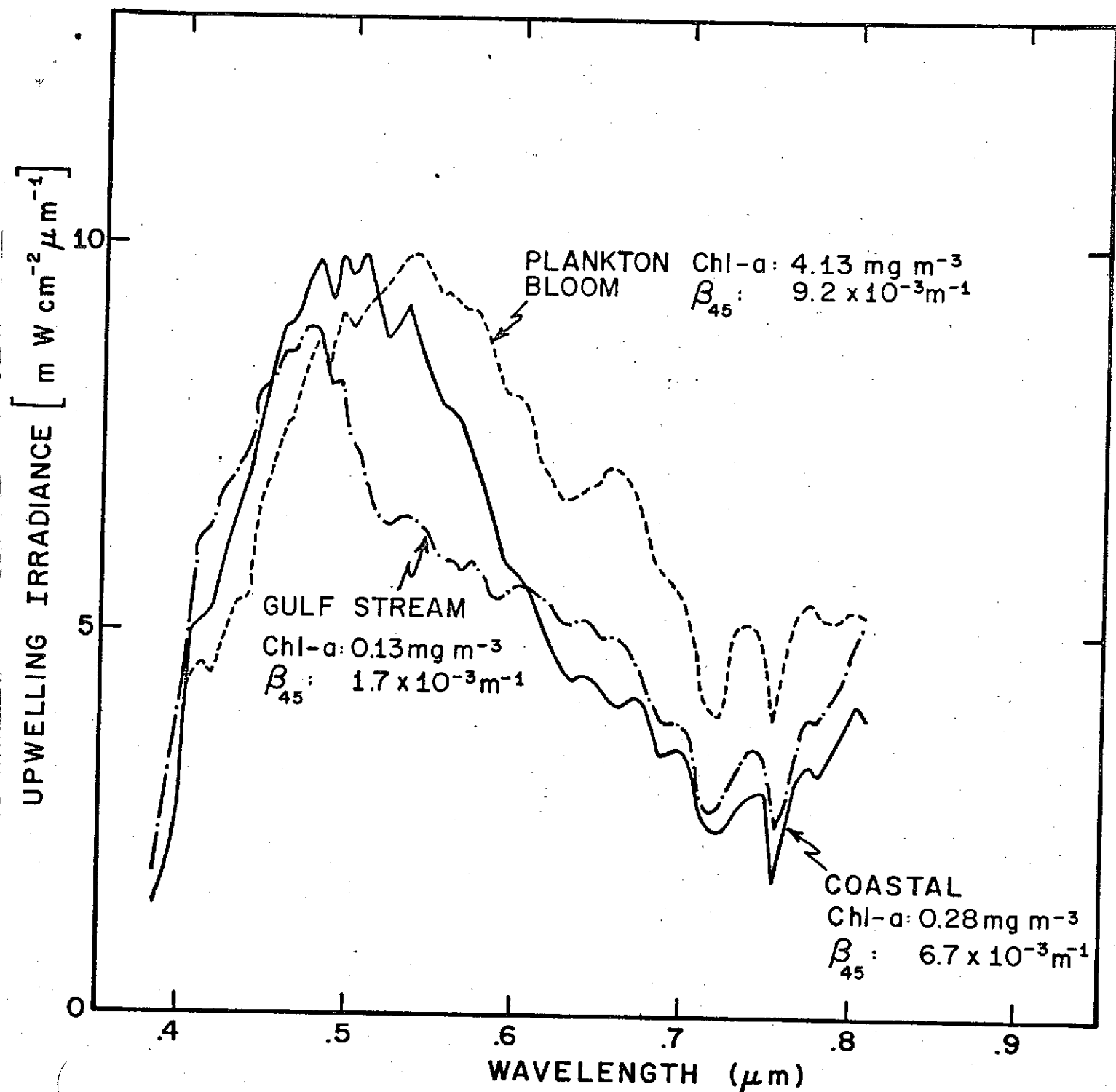
WAVELENGTH (μm)

Figure 12. Observed upwelling spectral irradiance in the Gulf of Mexico, November 1972. The three spectra represent typical observations during the time series, and show the shift of the dominant wavelength to larger values with increased surface chlorophyll-a. The volume scattering function, $\beta 45$, is for blue (436nm) light.
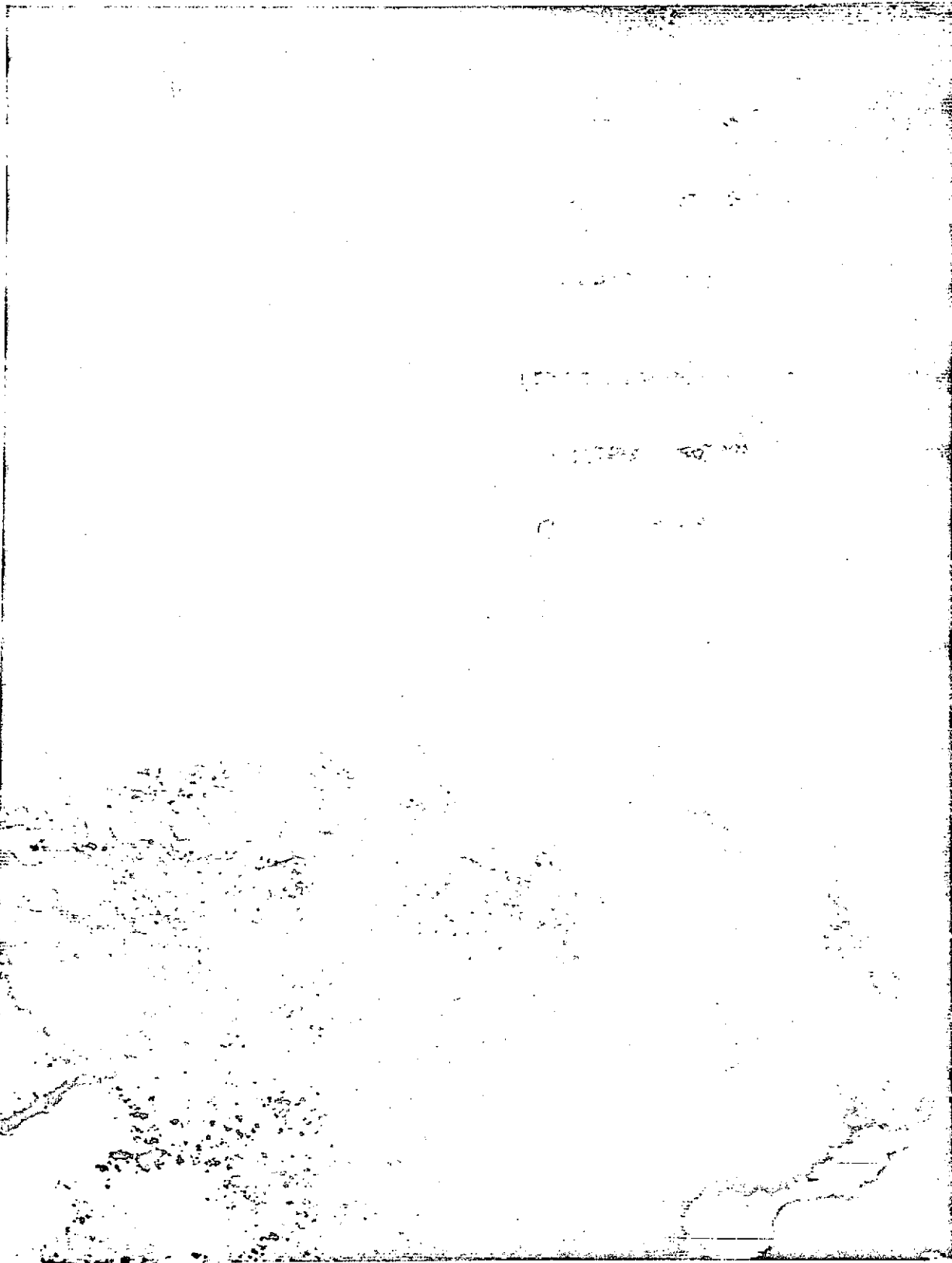
26

Figure 13. Negative print of computer contrast stretched (7<DN<15; n = 2) ERTS image of South Florida (ERTS ID 1026-15230). The Florida Current can be seen as a line of dark lineation parallel to the coast; bottom is essentially invisible in this MSS 6 scene. A ship can be seen by its characteristic V-shaped wake just offshore of Miami Beach. Possibly the Virginia Key sewer outfall area can be observed by its low reflectance due to an organic slick. Horizontal distance across the image is 90 kilometers.

27

REFERENCES

Chandrasekhar, S. (1960). Radiative Transfer, Dover, New York, 393 pgs.

Charnell, R. L., G. A. Maul, and R. M. Qualset (1973). Paper presented October 3, 1973, ASP-ACSM Fall Convention, Orlando, Florida.

Corwin, T. L. and H. R. Richardson (1974). Preliminary report to the Commandant of the Coast Guard on the Gulf of Mexico Cyanide Barrel Spill, Daniel H. Wagner Associates, Paoli, Pennsylvania 19301, 36 pgs.

Cox, C. and W. Munk (1954). J. Opt. Soc. Am., 44(11), pp. 838-850.

Gordon, H. R. (1973). Appl. Opt., 12, pp. 2804-2805.

Gordon, H. R. and O. B. Brown (1973). Appl. Opt., 12, pp. 1549-1551.

Gordon, H. R. (1974). To be published in J. Opt. Soc. Am.

Hansen, D. V. and G. A. Maul (1970). Remote Sensing of Environment, 2, pp. 161-164.

Jerlov, N. G. (1968). Optical Oceanography, Elsevier, New York, pg. 56.

Leipper, D. F. and D. Volgenau (1970). Transactions, A.G.U., 51(4), pg. 310.

Maul, G. A. and D. V. Hansen (1972). Remote Sensing of Environment, 2, pp. 109-116.

Maul, G. A. (1973a). Transactions, A.G.U., 54(4), pg. 310.

Maul, G. A. (1973b). Symposium on Significant Results Obtained from the Earth Resources Technology Satellite-1. NASA SP-327, Vol. I (B), pp. 1365-1375.

Maul, G. A. (1974a). COSPAR: Space Research XIV, pp. 335-347.

Mueller, J. L. (1973). PhD. Dissertation Oregon State University, Corvalis, Oregon, 239 numbered leaves.

Murphy, E., K. Steidinger, B. Roberts, J. Williams, and J. Volley (1973). Submitted to Limnology and Oceanography.

Petzold, T. J. (1972). Volume Scattering Functions for Selected Ocean Waters, Scripps Institution of Oceanography, Visibility Laboratory SIO Ref. 72-28, 82 pgs.

Preisendorfor, R. W. (1965). Radiative Transfer on Discrete Spaces, Permagon,
     New York, 462 pgs.

Tyler, J. E. and R. C. Smith (1970). Measurements of Spectral Irradiance Under-
     water, Gordon and Breach, New York, 103 pgs.

Tyler, J. E., R. C. Smith, and W. H. Wilson, Jr. (1972). J. Opt. Soc. Am.,
     62(1), pp. 83-91.